Hindawi
Geofluids
Volume 2021, Article ID 6689966, 16 pages
https://doi.org/10.1155/2021/6689966

Research Article

Deformation Behavior of Mining beneath Flat and Sloping Terrains in Mountainous Areas

Zhao Jianjun,[1] **Wan Xun**,[1] **Shi Yanbing**,[1] **Wei Jiangbo**,[2] **and Min Lee Lee**[3]

[1]*State Key Laboratory of Geohazard Prevention and Geoenvironment Protection, Chengdu University of Technology, 610059 Chengdu, China*
[2]*Shaanxi Provincial Key Laboratory of Geological Support for Coal Green Exploitation, Xi'an University of Science and Technology, 710054 Shaanxi, China*
[3]*Faculty of Science and Engineering, University of Nottingham Malaysia, 43500 Selangor, Malaysia*

Correspondence should be addressed to Zhao Jianjun; j.j.zhao@qq.com

Received 27 November 2020; Revised 9 January 2021; Accepted 27 January 2021; Published 19 February 2021

Academic Editor: Yi Xue

Slope structures and surface terrains are two significant factors affecting the deformation behavior of mining slopes in mountainous areas. This research is aimed at investigating the deformation characteristics of a mining slope wielding Particle Flow Code (PFC), with 9 different mining configurations (i.e., horizontal distance from extracted panel center to slope shoulder, $D = -200$ m, -150 m, -100 m, -50 m, 0 m, 50 m, 100 m, 150 m, and 200 m). A representative slope in Faer Town, Liupanshui City, Guizhou Province, China, was selected, which was characterized by soft and hard interbedded rock strata. The results indicated that the overlying rock mass tended to move towards the sloping surface with mining beneath sloping terrain, which brought an asymmetrical subsidence funnel, and formed a wider relative disturbance range on the slope surface. With the vertical subsidence increasing additionally, the stability of the overall slope deteriorated. A safe mining range should be proposed based on evaluating the time-dependent deformation behavior at the slope shoulder and the overall slope stability.

1. Introduction

Longwall mining is one of the most generally adopted underground mining methods, particularly in mining areas with relatively uniform and thick coal beds [1]. Surface subsidence is the leading form of mining-induced geological hazards which has caused various adverse effects to the environment [2, 3].

Analyzing the mechanism of ground movement and estimating their magnitudes and geometries have long been the main concerns in risk management of mining operations. A reliable prediction of ground subsidence caused by the mining operations remains a great challenge [4]. An extracted panel formed, the deformation of the overlying rock mass depends on many factors, i.e., bedding structure, thickness, strength, discontinuous geometric, mechanical characteristics of the panel, thickness of the mined coal seam, and width and length of the extracted panel [5–8]. In addition to the properties of the coal seams and the overlying rock masses, in situ stress conditions, groundwater conditions, terrain gradient, mining method, process of extraction, and distribution of pillars may all add complexity to the ground subsidence estimation [4, 9, 10]. The ground deformation induced by the mining operation is thus a multifactor coupling problem in temporal and spatial scales.

The prediction of ground subsidence can be performed by various methods, such as numerical simulation, physical modelling, influence function method, empirical approach, and analytical technique [10–14]. In addition, with the advancement in geographic information system (GIS) and remote sensing (RS) technologies, the spatial database can be constructed to analyze the shape and magnitude of the subsidence [15, 16]. The capability of GPS network application in measuring ground horizontal displacement has made great contributions to monitoring and early warning systems for mining-induced geological hazards [17]. Application of geophysical methods enables geologists to develop a comprehensive understanding of fracture evolution in

Table 1: Distributions of mining-induced geological hazards in Liupanshui City on different strata (data compiled by end of 2016).

Types of geological hazards	Main distribution strata											Total
	C_2hn	C_3mp	P_2l	P_2m+q	P_3l	$P_3\beta$	T_1f	T_1y	T_1yn	T_2g	E	
Landslide	1	1	4	0	86	2	73	1	3	1	0	181
Collapse	0	0	0	2	9	1	19	2	6	0	1	39
Surface subsidence	0	0	2	1	69	2	37	4	8	0	0	122
Ground fissure	0	0	0	1	3	0	4	3	1	0	0	12
Debris flow	0	0	0	0	2	0	0	0	0	0	0	2
Total	1	1	6	4	169	8	133	10	18	1	1	356

the overburden rock masses induced by shallow mining activities [18, 19].

Many researchers performed numerical and physical modelling to estimate the subsidence of complex ground profiles. The physical modelling normally has difficulties dealing with an in situ stress state of rock mass (i.e., effect of gravitational force), which can be only simulated by geotechnical centrifuge [20, 21]. Performing a large geotechnical centrifuge test, however, can be extremely costly. The numerical simulation has been widely used to analyze mining slopes with complex geometries and simulate discontinuous and nonlinear mechanical behavior of rock masses [4, 9, 22–27]. The Discrete Element Method (DEM) is an efficient tool for analyzing instability of jointed rock slope, as proven by numerous successful cases [28–30].

There were in total 356 incidents of geological hazards (refer to Table 1) reported in the mountainous area in Liupanshui City, Guizhou Province, southwest of China. By the end of 2016, most of the hazards occurred on the P_3l and T_1f strata. A typical mining slope named Jianshanying slope in Faer Town, Liupanshui City, was selected. Wielding Particle Flow Code (PFC) to analyze deformation behavior with underground mining operations.

2. Mechanisms of Mining-Induced Slope Instability

Numerous previous studies reported that slopes subjected to underground mining are prone to caving and landslides [31–34]. There were 2 main models of mining-induced slope failures: (1) progressive rock falls and caving failures, which cause nearly vertical cliffs [25, 35], and (2) rock masses extruded from the slope toe causing holistic instability [36]. With underground extraction performed beyond the slope shoulder, most instabilities are initiated [37, 38].

According to Salmi et al. [4], the surface topography has a considerable impact on the mechanisms of mining-induced slope instability. Mining in hilly and mountainous terrains usually increases the risk of slope failure. In addition, mining beneath sloping terrains imposes an additional threat on ground subsidence, which usually occurs near a valley [35]. The coal seam extracted beneath flat terrains, the rock masses above the extracted panel were fragmented and caved into the panel immediately, and the fragmented rocks tend to fill the void forming a goaf. As a result of ascending step-loading imposed by the upper caving block, the stiffness of rock mass increases gradually [39]. The overburden strata remain intact and bend towards the extracted panel [40]. Owing to the expansibility of rock, the rock masses falling into the panel are subjected to lateral forces from the virgin strata, which rise gradually with the increase of depth and reach the maximum value at the coal pillar [41]. The boundary conditions on both sides of the extracted panel are identical, and hence, the magnitude and direction of lateral forces are completely symmetrical. Under the circumstances, there are different horizontal deformations in the rock masses, and it causes a symmetrical subsidence funnel on the surface [42]. In an extraction performed near or beneath a cliff, the lateral forces induced above the goaf (directed from the plateau towards the valley) are not counterbalanced by an identical force in the opposite direction. The rock mass near the valley has a greater horizontal displacement, and hence, an asymmetric subsidence funnel occurs on the slope surface.

The magnitude and shape of the surface subsidence, which is induced by mining operations under the condition of flat terrains, have been studied extensively. The localized deformation and overall instability constitute much more uncertainties attributed to the complex combination of terrains and structures in the sloping terrains. Studies on ground subsidence induced by mining activities in sloping terrains are still very limited. Several previous case studies of large-scale slope failures induced by mining include the Zhangjiawan collapse and Madaling landslide in Guizhou, China [36], and one of the largest contemporary landslides and mass movements reported at Nattai North, Australia [43], have drawn the global attention on the mass movement caused by mining activities and provoke the present study to be carried out.

This research is rooted in the exploration of mining-induced subsidence rules in P_3l and T_1f with Liupanshui City, Guizhou Province, China, as the typical. To be detailed, this research innovatively proposed 9 mining configurations for expounding the deformation behavior of mining beneath flat and sloping terrains by wielding Particle Flow Code, which is applied to the soft and hard interbedded and jointed slopes in the mountainous area. Furthermore, the time-dependent deformation was measured at the slope shoulder, as the transition part of the flat and sloping terrains, to propose a safe mining range, which was meaningful in the risk management of mining operations.

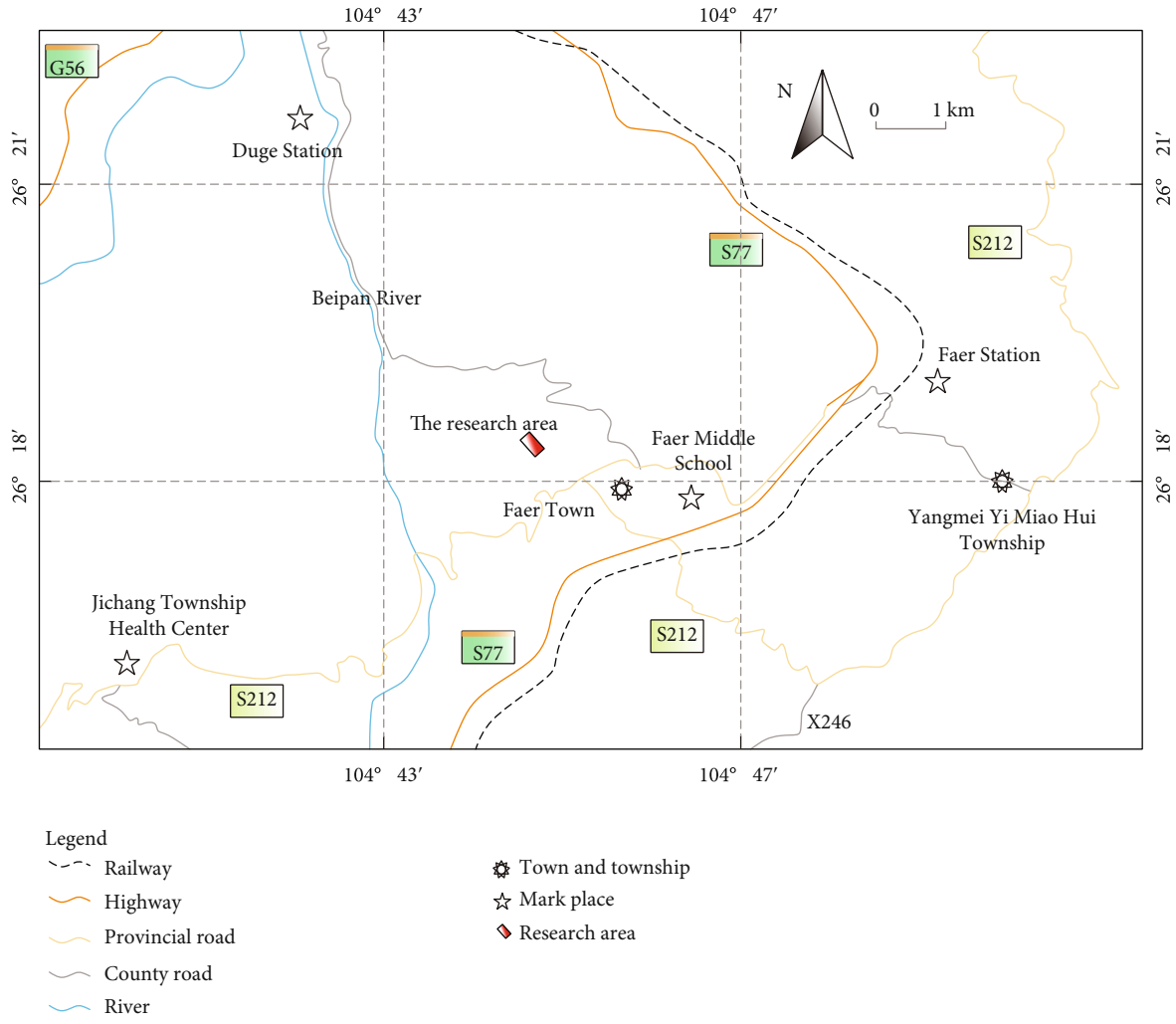

Figure 1: Location of study area.

3. Case Study

3.1. Model Development. Liupanshui City in Guizhou Province, China, is known for its proven coal resources and reserves. The city which is known as the "Southwest Coal Sea" has developed multistage coal seams on the P_3l stratum. In 2015, there were more than 800 mines in the city, while more than 400 landslide and ground subsidence incidents have been reported, which were mainly caused by improperly planned mining activities. In the present study, a mining slope named Jianshanying slope in Faer Town, Liupanshui City, was selected as the case study. The specific geographical coordinates of the study area are E104°44′11″ and N26°18′20″ (Figures 1 and 2).

In the western part of the Guizhou plateau, a low mountainous terrain was formed because of the tectonic erosion. Typically, both steep and gentle structures were formed in the mining slope. Most of the coal-bearing strata are located in the flat terrains, while the interbedded sandstone and mudstone are mainly located in the sloping terrains. The surface terrain of the Jianshanying slope was reasonably generalized to simplify the subsequent numerical modelling processes. Three sets of dominant joints were considered in each strata, and one set has the same tendency as the strata. The general stratifications of the slope are presented in Figure 3. Coal and mudstone formed the relatively weak strata in the slope, however, the effect of the stratified structure was not considered in them.

Mining slopes are typically prone to time-dependent failures in the form of ground subsidence and slope sliding [44]. After going through a long process of mining, 6 coal layers had been mined out beneath the Jianshanying mining slope forming a total of 13 mining panels. These mining activities had caused severe impact on the stability of the slope. To simplify the analysis, the present study only focused on the impact of mining with the first coal layer on the slope instability. Nine mining configurations with different horizontal distances (D) from the extracted panel center to slope shoulder (where the flat terrain intersected with the sloping terrain) were set, namely, $D = -200$ m, -150 m, -100 m, -50 m, 0 m, 50 m, 100 m, 150 m, and 200 m (see Figure 4 and Table 2). The width of each extracted panel along the strata dip direction was within the range of 150~250 m, while the thickness of the coal seam was ranging from 2 to 4 m in

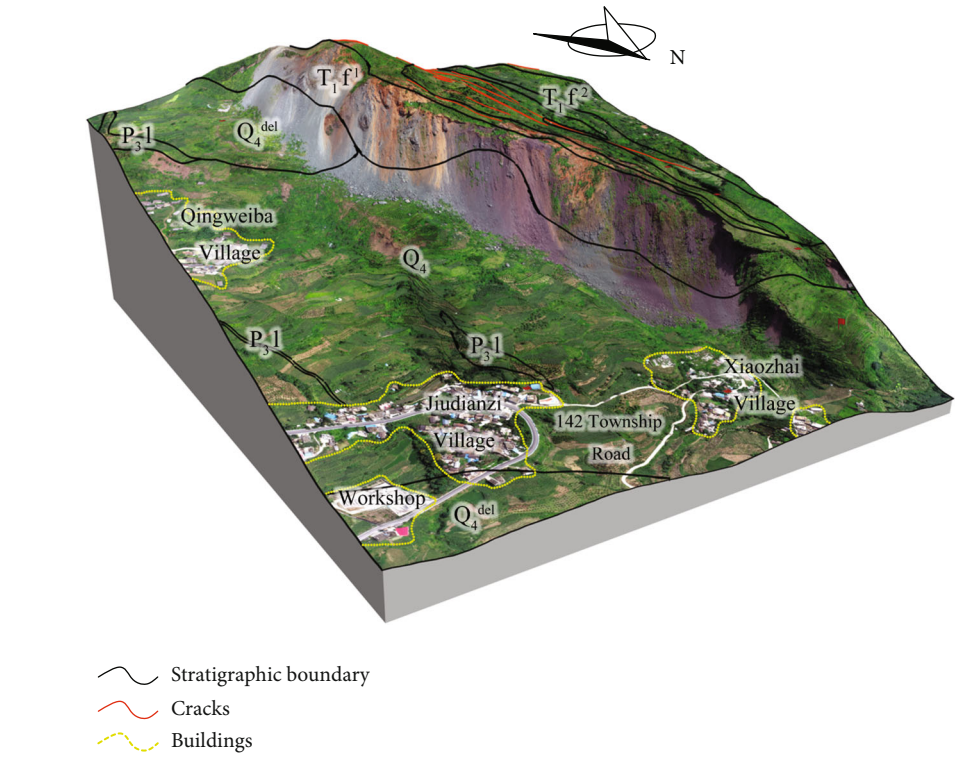

Figure 2: 3D terrains of Jianshanying mining slope.

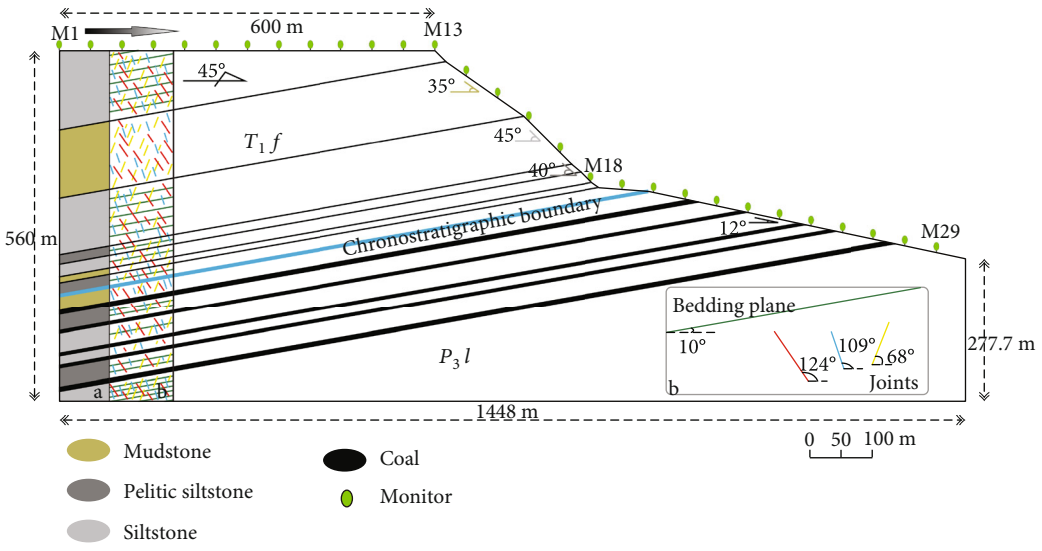

Figure 3: Generalized profile of mining slope model ("T_1f" is Feixianguan group and "P_3l" is Longtan group).

statistics. The width of the extracted panel and the thickness of the mined-out coal seam were fixed at 200 m and 6 m in practice. The above configurations were set to systematically study the influences of extracted panel depth, horizontal distance between the center of extracted panel and slope shoulder, and surface terrain condition on the instability of the mining slope. The extracted panel was located beneath a flat terrain with $D \leq -100$ m, while the extracted panel was beneath a sloping terrain with $D \geq 100$ m (Figure 4). A total of 29 monitoring points with a horizontal interval of 50 m were set in the numerical model, for revealing the deformation characteristics of the slope surface with various configurations.

3.2. Particle Flow Code. Rock masses are discontinuous medium, and hence, the use of the DEM is justifiable [4]. PFC (Particle Flow Code), a popular program based on the DEM, is widely used to simulate the macroscopic characteristics of rock-soil masses. The soil/rock aggregates are modelled as either rigid disks (2D) or spheres (3D), and they are

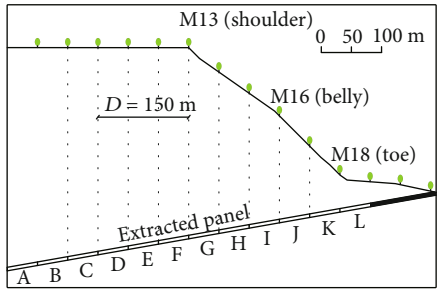

Figure 4: Mining configurations considered for numerical simulation.

connected by specific contact models as an equivalent model of rock-soil mass [45]. The PFC adopts the time step iterative calculation method (Figure 5). Newton's second law and the law of force and displacement are repeatedly applied in the calculation for updating the motion state of units in real-time, and the contact force and torque between the updated units are further determined by the force-displacement relationship [46].

The law of force-displacement reflects the contact relationship between particles, also the relationship between the contact force and relative motion. In the PFC model, the contact force ball-ball and ball-wall can be divided into normal force and transverse force (Equation (1)). The particles move and rotate under the action of unbalanced forces and unbalanced torques (Equations (2) and (3)). The motion equation of PFC is solved using the centered finite difference method in relation to time step (Δt). The translational and rotational acceleration ($\ddot{x}_i^{(t)}$ and $\dot{\omega}_i^{(t)}$) of particles at any time can be obtained from Equations (4) and (5). The translational velocity ($\dot{x}_i^{(t)}$), angular velocity ($\omega_i^{(t)}$), and displacement ($x_i^{(t)}$) of particle motion can be obtained from equation transformation (Equations (6), (7), and (8)). The definitions of the model parameters are summarized in Table 3:

$$\overrightarrow{F_i} = \overrightarrow{F_i^n} + \overrightarrow{F_i^s}, \tag{1}$$

$$\overrightarrow{F_i} = m\left(\overrightarrow{\ddot{x}_i} - \overrightarrow{g_i}\right), \tag{2}$$

$$\overrightarrow{M_i} = \overrightarrow{\dot{H}_i}, \tag{3}$$

$$\ddot{x}_i^{(t)} = \frac{1}{\Delta t}\left(\dot{x}_i^{(t+\Delta t/2)} - \dot{x}_i^{(t-\Delta t/2)}\right), \tag{4}$$

$$\dot{\omega}_i^{(t)} = \frac{1}{\Delta t}\left(\omega_i^{(t+\Delta t/2)} - \omega_i^{(t-\Delta t/2)}\right), \tag{5}$$

$$\dot{x}_i^{(t+\Delta t/2)} = \dot{x}_i^{(t-\Delta t/2)} + \left(\frac{F_i^{(t)}}{m} + g_i\right)\Delta t, \tag{6}$$

$$\omega_i^{(t+\Delta t/2)} = \omega_i^{(t-\Delta t/2)}\Big) + \left(\frac{M_i^{(t)}}{I}\right)\Delta t, \tag{7}$$

$$x_i^{(t+\Delta t)} = x_i^{(t)} + x_i^{(t+\Delta t/2)}\Delta t. \tag{8}$$

3.3. Rock Mass Parameters. In particle flow simulation, the macroscopic mechanical behaviors of the rock and soil masses are governed by the microscopic mechanical properties of particles, nevertheless, there is a highly nonlinear relationship between them. Typically, the transformations of the macroscopic and microscopic parameters are carried out by means of biaxial compression tests [47]. The most common set of siltstone and pelitic siltstone was selected for parameter calibration to avoid the discreteness of rock samples. The stress-strain curve obtained from the PFC simulation under the condition of no confining pressure was reasonably consistent with that of the laboratory (Figure 6). Both siltstone and pelitic siltstone showed significant brittle failure characteristics. The initial balance was carried out after gravity loading in the process of engineering scale simulation, and the increment of displacement and velocity during the process was cleared, and hence, the consistency of the stress-strain curve in the compaction stage was superfluous. The elastic modulus (E) and unconfined compressive strength (UCS) of siltstone and pelitic siltstone obtained from the laboratory and PFC are shown in Table 4; moreover, the fitting degree of their magnitude values is a measure index of calibration. Both mudstone and coal retrieved in the field had great discreteness with mechanical properties, which obstructed calibration by the PFC test. This research attempted to bring empirical values to the parameters of coal and mudstone, and the full mining model simulation was used in comparison with the actual situation. The parameter inversion method was used to adjust the rock block parameters as empirical.

The mechanical parameters of rock masses are generally smaller than those of intact rock with laboratory scale because of the size effect and discontinuity of rock masses [48]. Practically, the effects of bedding plane and dominant joints are often considered in simulation, and the equivalent jointed rock masses technology is applied. The smooth-joint model was chosen over the flat-joint model, which is poor in simulating the plane dilation mechanics, to reflect the constitutive relation. Furthermore, the smooth-joint model enabled the joint properties to a limited range on both sides of them, and a random joint model was formed to verify and correspond to the characteristics of the slope on-site. For this purpose, based on the laboratory mechanical experimental results, numerical simulation calibration testing, and the equivalent rock masses technique, the full mining model (the six-coal-seam mining model) simulation was used in comparison with the actual situation, which ensured that the simulation outputs were reasonably consistent with the actual field deformation (i.e., occurrence of deposition at the slope toe, presence of tensile cracks in the middle of the slope, and subsidence at the edge of slope), which was acquired through the UAV survey (Figure 7). In this paper, parameters related to rock and soil masses materials were obtained and adjusted by parameter inversion. The calibrated microscopic mechanical parameters of the rock masses, which were adopted for the PFC simulation of the Jianshanying mining slope, are summarized in Table 5.

Table 2: Details of mining configurations.

D (m)	-200	-150	-100	-50	0	50	100	150	200
Extracted panels	$A+B+C+D$	$B+C+D+E$	$C+D+E+F$	$D+E+F+G$	$E+F+G+H$	$F+G+H+I$	$G+H+I+J$	$H+I+J+K$	$I+J+K+L$
Panel depth (m)	345.5	336.6	328	319.2	310.1	261.5	217.1	170.9	112.1

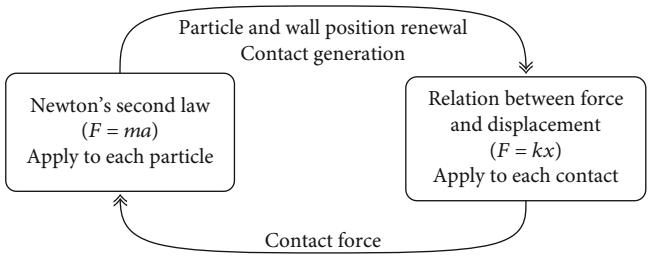

Figure 5: Workflow of PFC analysis.

Table 3: Definitions of symbols.

Symbol	Definition	Symbol	Definition
F_i	Contact force	$\dot{x}_i$	Translational velocity
F_i^n	Normal contact force	x_i	Displacement
F_i^s	Shear contact force	$\dot{\omega}_i$	Slew acceleration
g_i	Gravitational acceleration	ω_i	Angular velocity
M_i	Unbalance moment	I	Inertia moment
$\ddot{H}_i$	Angular momentum	Δt	Time step
$\ddot{x}_i$	Translational acceleration	m	Particle quality

4. Results of Numerical Analysis

4.1. Evaluation of Crack Propagation. In the panel extracted, tensile cracks initiated to propagate in the overburden materials. The cracks mainly aggregated at the boundary of the extracted panel and extended up to the surface [49]. Obviously, tensile cracks were observed beneath the slope shoulder with $D = -100$ m. The panel was extracted directly below the slope shoulder ($D = 0$ m); the tensile cracks had developed in front of the slope shoulder and extended to the sloping terrain (Figure 8(e)). These results implied that there was an "aggregation" on the extension of tensile cracks beneath the slope shoulder.

According to Salmi et al. [50], neglecting the effect of stratum bedding in simulating mining-induced subsidence in flat terrains would yield a wider but shallower subsidence trough as compared with the field conditions. Therefore, the strata bedding surface and joints should be carefully modelled to improve the simulation outputs (Figure 3).

The sum of upside and downside crack angles ($\gamma + \beta$) was wielded to characterize the relative disturbance range of overburden rock masses. The term "relative" was used to indicate that the thickness of rock strata, which is above the extracted panel, was not taken into consideration. A low value of "$\gamma + \beta$" indicated a large relative disturbance range, and vice versa (refer to Figure 9). The extracted panel is partially or completely located beneath the sloping terrains; the relative disturbance ranges for the cases were greater than those beneath the flat terrains. With the upside crack angle decreasing, the subsidence trough of the latter was wider than that of the former (see in Figure 8). Moreover, the propagations of tensile cracks at the extracted panel boundary were almost parallel with all mining configurations. The crushing of the coal pillar resulted in an increment in the distance between the position of boundary tensile cracks and the center of the extracted panel and hence altered the crack angle (Figure 10). The center of the extracted panel positioned in front of the slope shoulder; the otherness between upside and downside crack angles increased. The upside crack angle reached the minimum value of 64°, and the summation angle of "$\gamma + \beta$" reached the minimum value of 151° with $D = 0$ m; moreover, the rock masses above the extracted panel were disturbed to the greatest.

4.2. Evaluation of Horizontal Displacement. Coal mining causes significant vertical deformations. For materials which are characterized by low compactness and high expansibility in the subsidence area, the lateral compression of the strata surrounding the extracted panel would increase and cause an expansion to the sloping terrains. Subsidence immediately causes lateral deformation with the constraining forces of surrounding rock mass. A lower confining pressure makes the effect of lateral deformation more prominent [41]. Therefore, symmetrical and high constraining forces make the lateral deformation inappreciable [51]. In sloping terrains, the overburden rock masses produce relatively low lateral constraining forces, which are insufficient to offset the dilatational forces of rock masses caving into the panel. As a result, the disturbed rock mass would displace towards the sloping terrains (Figure 10). The extraction panels are located at different positions; Figure 11 shows the lateral deformations of rock masses. The lateral deformation of overburden rock mass above the extracted panel was not symmetrical, with flat-sloping terrains as simulated. The lateral deformation beneath the flat terrain side was lower than that of the sloping side. The extraction panel was located close to the sloping terrain; the lateral deformation was intensified and caused an outcrop towards the sloping surface.

Bedding planes provided a suitable path for lateral movement of strata in both flat and sloping terrains. A bedding plane, with a low bonding strength, provided less resistance in the direction of the overburden material movement and hence caused the sliding between the layers. The "zigzag" horizontal displacement change zone can be seen in Figures 11 and 12.

Interestingly, lateral deformations towards the slope inner part were observed in the mudstone layer with $D < 100$, with

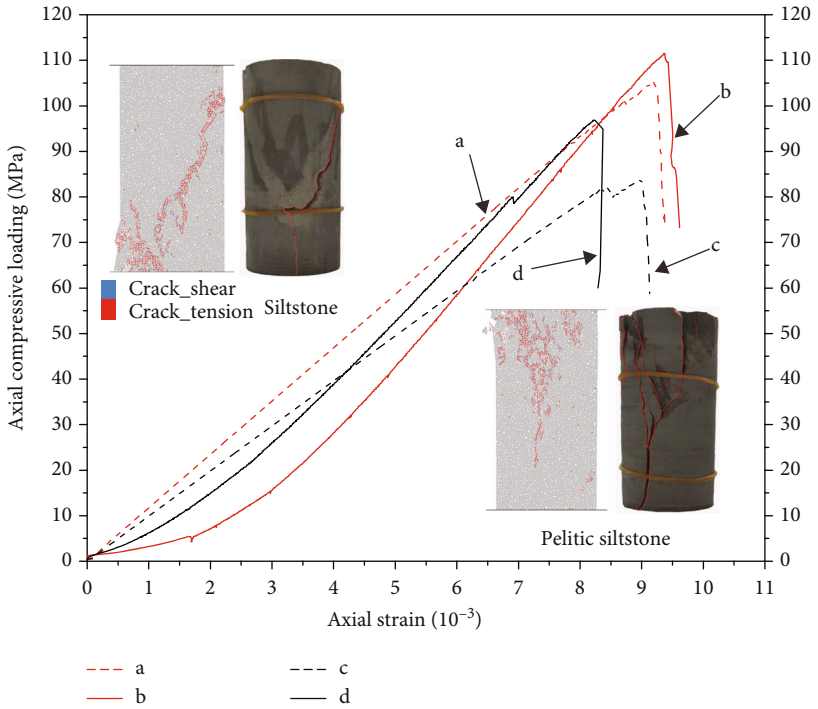

Figure 6: Stress-strain curves obtained from uniaxial compression tests (red lines: (a, b) represent siltstone; black lines: (c, d) represent pelitic siltstone. Solid lines are results obtained from laboratory tests, while dashed lines are results obtained from PFC calibration test).

Table 4: Uniaxial compression test results.

Parameter	Siltstone		Pelitic siltstone	
	Laboratory test	PFC test	Laboratory test	PFC test
E (GPa)	15.75	11.44	13.6	9.35
UCS (MPa)	111.49	105.26	96.87	83.76

the maximum value reaching 0.98 m (Figure 12(b)). However, there was no similar phenomenon in the mudstone directly above the extracted panel (Figure 11). With the in situ stress releasing, the materials at the slope shoulder poorly cemented were further loosed. Holding a more complete and dense layered structure, the siltstone and pelitic siltstone were subjected to stick-slip resistances along the bedding plane in the lateral motion. Conversely, the resultant force, including the gravitational force, redistributed stress, and the cementing force between the materials, leading to the deformation of mudstone.

A potential through slip plane appeared on the slope with $D = -100$ m (Figure 11(c)), which was initiated from the inner boundary of the extracted panel, extended upward to the goaf and the thin mudstone layer, and subsequently spread from the outer boundary of the extracted panel to the toe of the slope, causing the overall instability of slope. A horizontal displacement was observed of 0.4 m at the toe.

4.3. Evaluation of Surface Subsidence. The maximum surface subsidence is consistently located above the inner part of the extracted panel under various mining configurations in the countertilt slope. Furthermore, the sloping surface

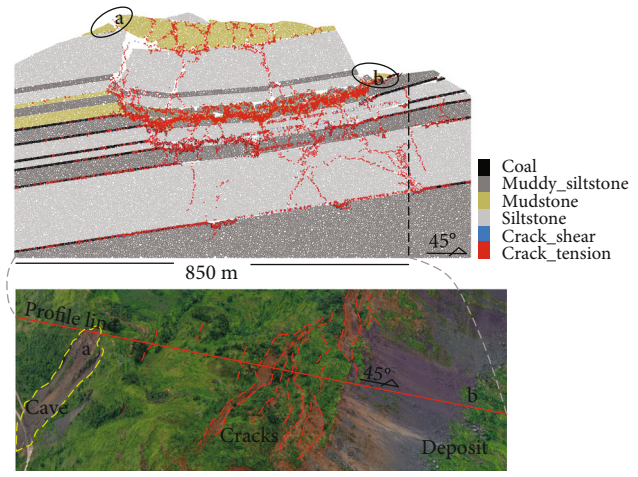

Figure 7: Comparisons of a typical PFC simulated deformation and the actual field observation.

with thinner overburden materials has a larger maximum subsidence area, as indicated by the cases of $D \geq 0$ m (Figure 13(a)). These results proved that the slope has reached the "sufficient mining conditions" with $D \geq 0$ m. For obtaining the increment in surface subsidence beneath the sloping terrains, the maximum subsidence (W_0) of flat terrains was brought to the present research, which was referred to Equation (9) proposed by Zou [52] under the "sufficient mining conditions":

$$W_0 = qm \cos \alpha, \tag{9}$$

Table 5: Microstrength parameters used for PFC simulations.

Parameter	Definition	Siltstone	Pelitic siltstone	Mudstone	Coal
R_{min}	Minimum particle radius (m)	1.6	1.6	1.2	0.8
R_{max}/R_{min}	Particle radius ratio, uniform distribution	1.25	1.25	1.33	1.5
ρ	Particle density (kg/m^3)	2850	2650	3050	1850
E_c	Interparticle contact modulus (GPa)	7	6	2	2
K	Normal-to-shear stiffness ratio	1.8	2	2.2	2.4
μ	Microfriction coefficient	0.3	0.38	0.75	0.58
E_c'	Bond effective modulus (GPa)	7	6	2	2
K'	Bond normal-to-shear stiffness ratio	1.8	2	2.2	2.4
σ_c	Parallel bond normal strength (MPa)	35	30	10	9
τ_c	Parallel bond shear strength (MPa)	35	30	10	9
K_j	Joint stiffness ratio		1		
μ_j	Joint microfriction coefficient		0.35		

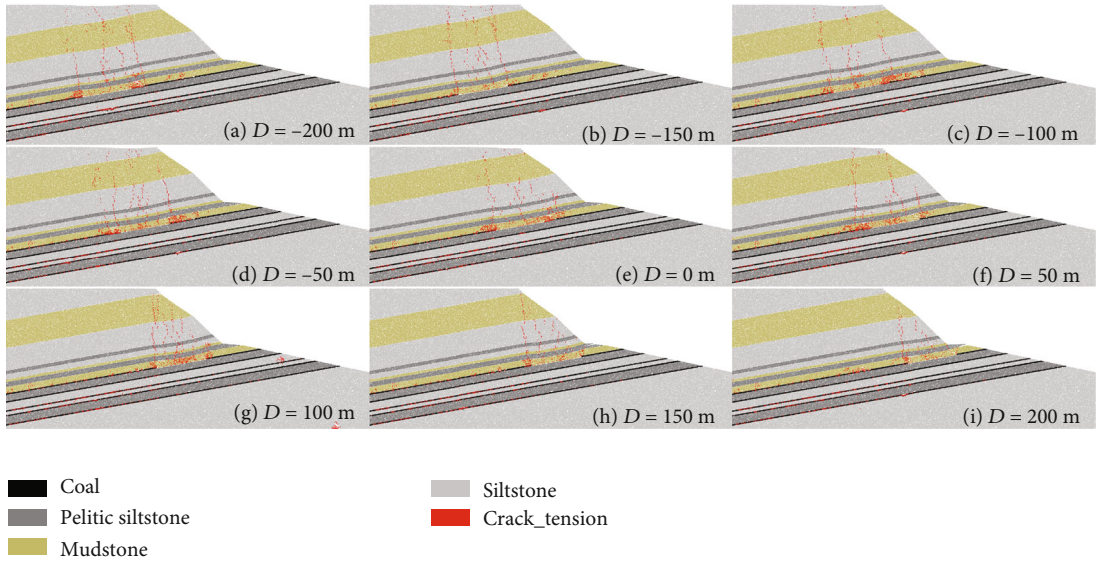

Figure 8: Crack propagations after coal seam extractions with different mining configurations.

where q is the subsidence coefficient under the "sufficient mining conditions," m is the thickness of the mining coal seam, and α is the dip angle of the coal seam.

Wielding the lithology comprehensive evaluation index (p) to characterize the degree of influence of lithology on surface subsidence [52]:

$$p = \frac{\sum_1^n h_i Q_i}{\sum_1^n h_i}, \tag{10}$$

where h_i is the thickness of overburden rock strata and Q_i is the lithologic classification index of overburden rock mass. The value of Q_i ranges from 0 to 1 for the first mining slope according to the hardness of the lithology. The Q_i values for the coal seam, mudstone, pelitic siltstone, and siltstone in this research were set at 0.9, 0.8, 0.4, and 0.05, respectively.

Based on the comprehensive evaluation index of lithology (p), the subsidence coefficient (q) of flat terrains under the "sufficient mining conditions" can be acquired by the following:

$$q = 0.45 + 0.5p. \tag{11}$$

From the above computations, W_0 for the 5 mining configurations with $D \geq 0$ m were 3.761 m ($D = 0$ m), 3.702 m ($D = 50$ m), 3.436 m ($D = 100$ m), 3.126 m ($D = 150$ m), and 3.294 m ($D = 200$ m). Accordingly, the increment in subsidence of sloping terrains as compared with the flat terrains was 2.761 m, 2.822 m, 3.101 m, 2.836 m, and 2.424 m, respectively.

Khanal et al. [53] suggested that the ratio of subsidence to thickness of overburden rock mass (S/T) could be positively correlated with the width to depth ratio of the mine (W/D_1). In this research, the thickness (T) and width (W) were fixed at 6 m and 200 m, respectively. The findings from the mining

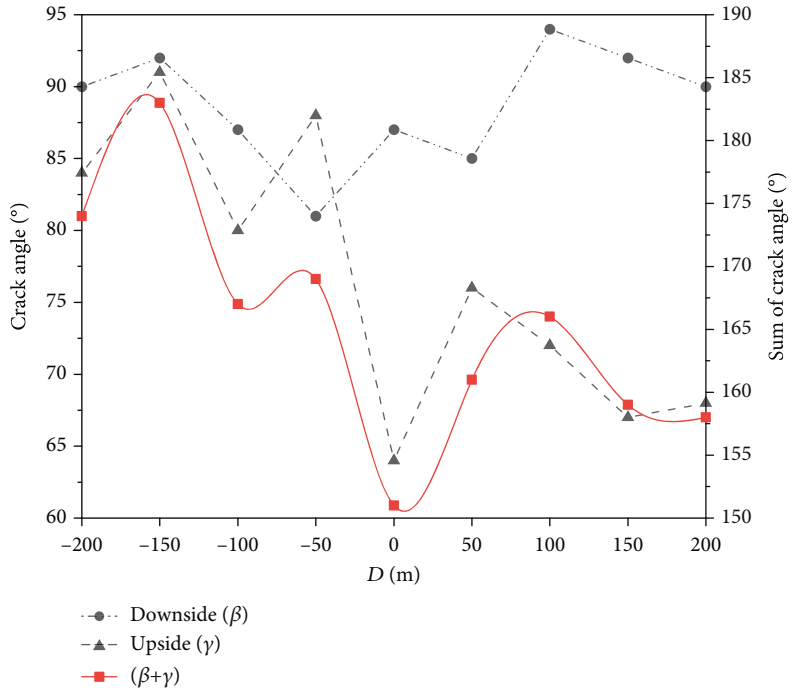

Figure 9: Changes in crack angle for different mining configurations.

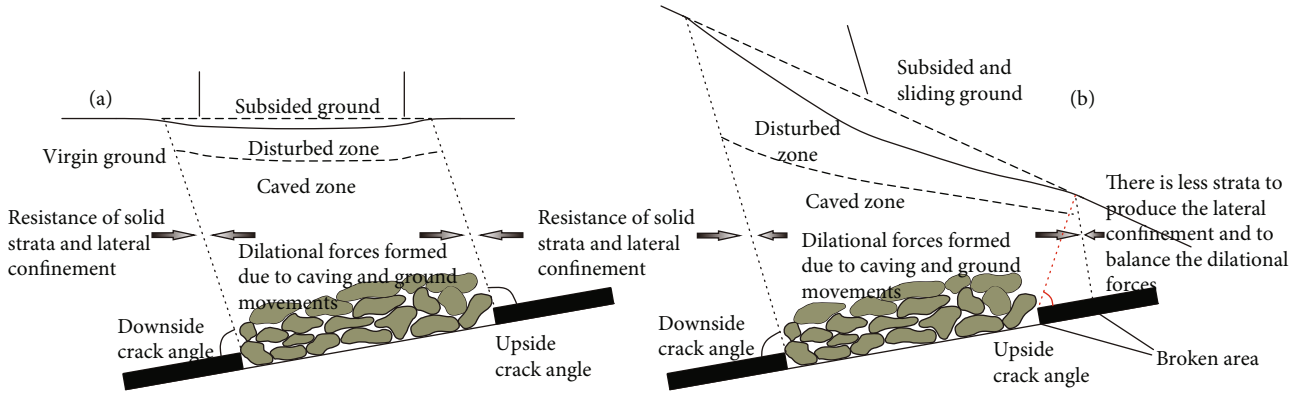

Figure 10: Mechanical mechanisms of mining-induced subsidence in (a) flat terrains and (b) sloping terrains (adapted from [41]).

configurations of $D < 100$ m showed consistency with that of Khanal et al. [53], but an opposite trend was observed with $D > 100$ m (Figure 13).

4.4. Evolution of Deformation at Slope Shoulder. The deformation behavior of the slope shoulder, a transition from flat terrains to sloping terrains, has been focused on in this research. The monitoring data of M13 was selected to characterize the deformation of rock mass at the slope shoulder. Figures 14–17 present the vertical and horizontal deformation characteristics of the rock mass over time under short-term and long-term conditions, respectively. The following findings are reported from the analyses:

(a) Short term

(i) Initiating the horizontal displacement and subsidence concurrently at the time step of 3000 with various mining configurations, which indicated that both the horizontal displacement and subsidence occurred right after the formation of the extracted panel

(ii) The extracted panel is located below the slope shoulder (-100 m $\leq D \leq 100$ m); the subsidence rate and value at the slope shoulder were higher than that in flat terrains

(b) Long term

(i) The rock mass at the slope shoulder showed prominent horizontal displacement (1.23 m) and subsidence (6.52 m) with $D = 0$ m and 50 m

(ii) The time required to stabilize the deformation at the slope shoulder was longer in flat terrain mining

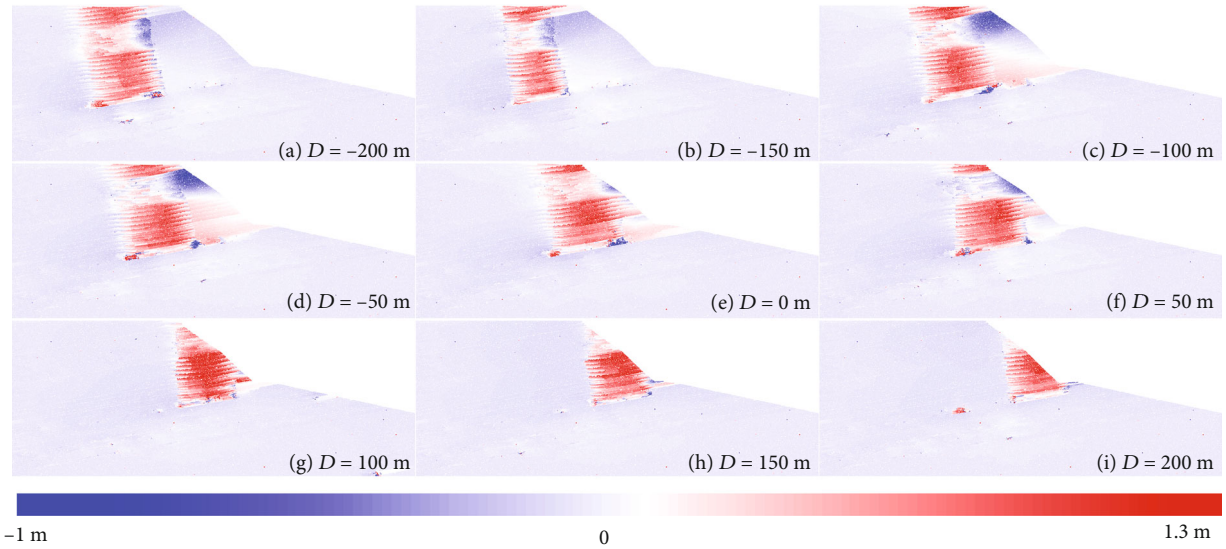

Figure 11: Contours of horizontal displacements after coal seam extractions with different mining configurations.

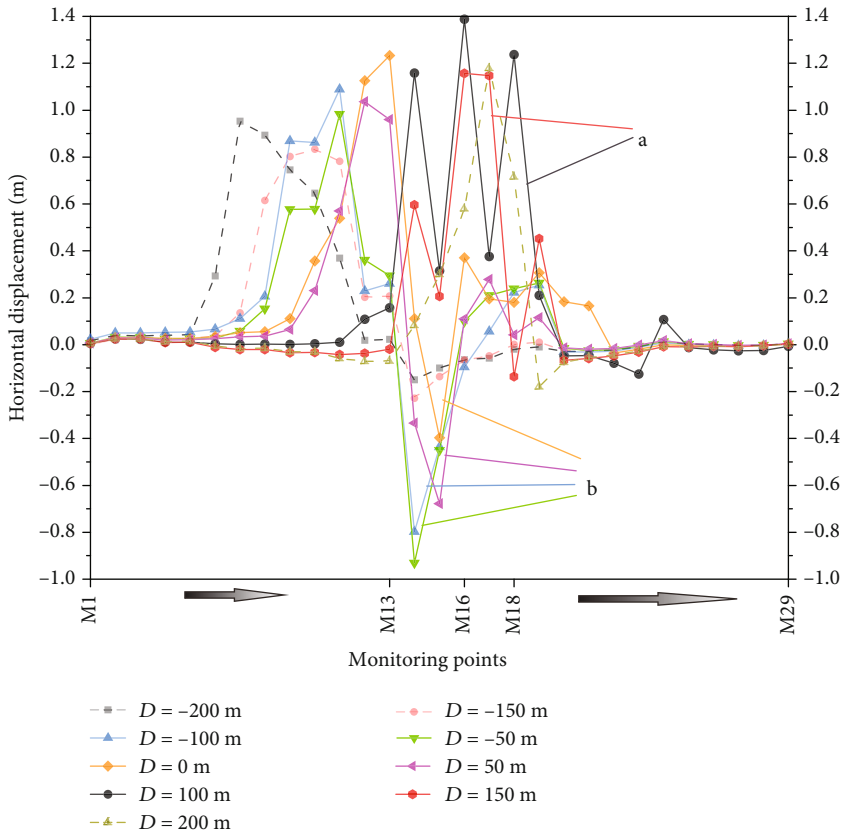

Figure 12: Horizontal displacement at the ground surface for different mining configurations.

(iii) The rock mass at the slope shoulder initially displaced horizontally towards the inner part and, subsequently, displaced outwards to the slope facing with $D < 0$ m. The horizontal displacement behavior depended on the location of the inner boundary of the extracted panel with $D \geq 0$ m. The rock mass at the slope shoulder displaced horizontally towards the direction of the slope facing with $D = 0$, 50, and 100 m. Observing a lower or negligible value with $D \geq 100$ m, which was identical to the cases of $D < 0$ m in the pattern of rock mass displacement

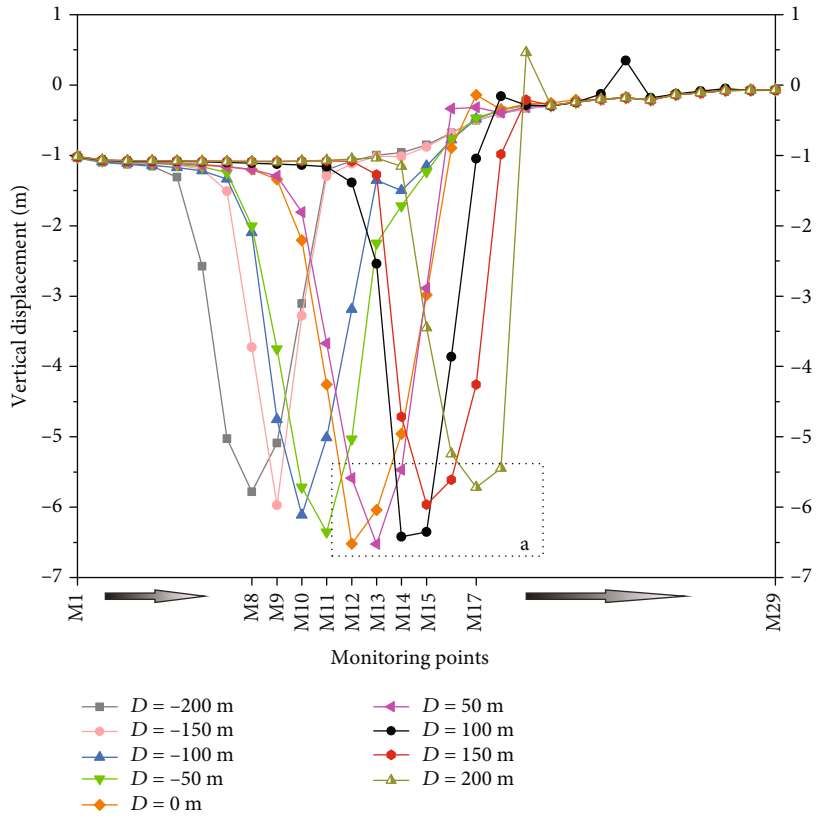

Figure 13: Vertical displacement at the ground surface for different mining configurations.

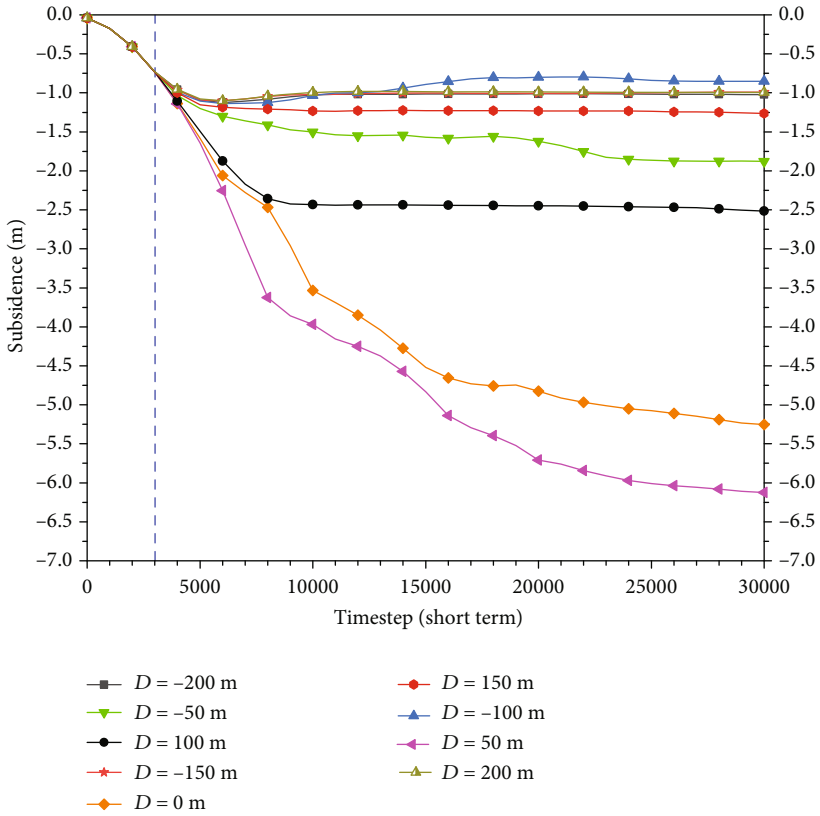

Figure 14: Variations in vertical displacement over time at slope shoulder for different mining configurations (short-term condition).

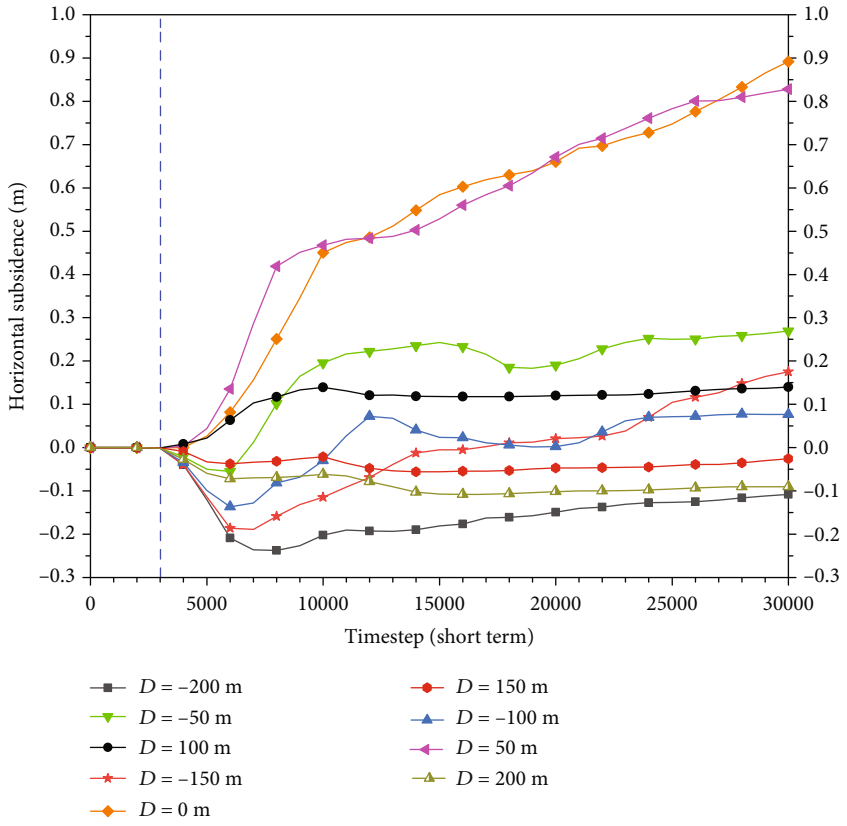

Figure 15: Variations in horizontal displacement over time at slope shoulder for different mining configurations (short-term condition).

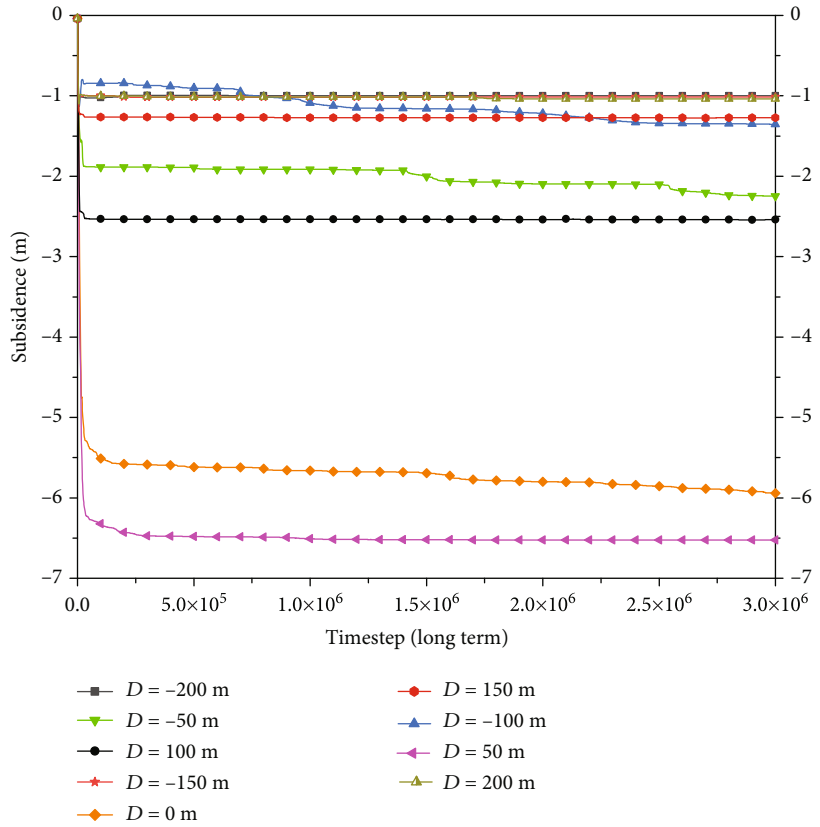

Figure 16: Variations in vertical displacement over time at slope shoulder for different mining configurations (long-term condition).

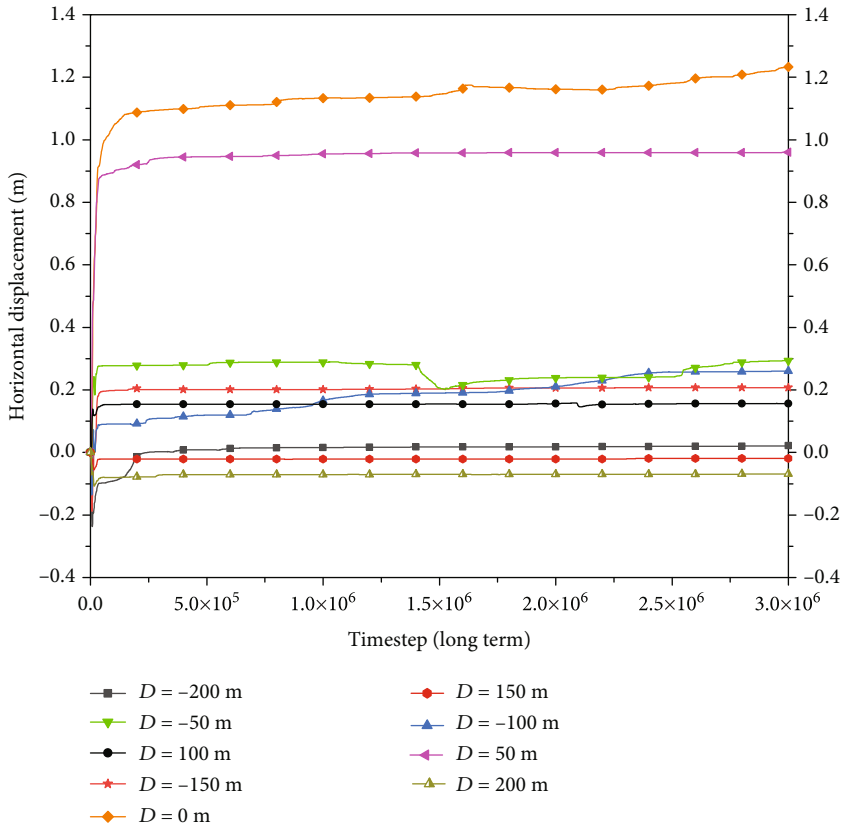

Figure 17: Variations in horizontal displacement over time at slope shoulder for different mining configurations (long-term condition).

5. Discussion

This research investigated the mechanical mechanisms of mining activities in flat and sloping terrains, with the considerations of deformation of overburden rock masses and propagation of tensile cracks. A model was established based on the typical mining-induced slope structure of a case study in southwest China. To the authors' knowledge, this is the first research reported on the use of PFC for analyzing the mining slope deformation behavior, with the extracted panel located beneath various complex terrains (i.e., flat terrain, slope shoulder, and sloping terrain). The time-dependent deformation characteristics of the rock mass at the slope shoulder were studied in detail. The sum of upside and downside crack angles was proposed to characterize the relative disturbance range of overburden rock mass, and reasonable and safe configurations of single-layered mining operations in mountainous areas were put forward.

It should be noted that the findings from the present research were handicapped by several limitations, such as the width of the extracted panel along the inclined strata was remained constant at 200 m, and the interval of two adjacent extracted panels in all mining configurations was kept at 50 m. In addition, the microstrength parameters of coal and pelitic siltstone were not derived from the uniaxial compression simulation by the PFC. Owing to these limitations, the functional relationship between surface subsidence and geological and geotechnical factors cannot be fully revealed in this research. These issues can be solved if the following future improvements are taken: (i) setting the extracted panel width as an independent variable and shortening the interval, (ii) increasing the number of samples for coal and pelitic siltstone and acquiring the mechanical parameters by wielding the support vector machine (SVM) coupled with the microstrength parameters by PFC, and (iii) setting the number of configurations of mining in sloping terrains to be 5 to 10 times of independent variables, for finding the regression relationship between the maximum subsidence and geological and geotechnical factors.

6. Conclusion

The present research investigated the deformation behavior of slopes under different mining configurations (i.e., horizontal distance from extracted panel center to slope shoulder, $D = -200$ m, -150 m, -100 m, -50 m, 0 m, 50 m, 100 m, 150 m, and 200 m) by wielding PFC. The Jianshanying mining slope, which was generalized based on the actual field investigation and laboratory experiment data, in Faer Town, Shuicheng county, Guizhou Province, was selected. Based on the laboratory mechanical experimental results, numerical simulation calibration testing, and the equivalent rock mass technique, the full mining model (the six-coal-seam mining model) simulation was used in

comparison with the actual situation, which ensured the rationality of microstrength parameters of rock masses and joints. The following conclusions can be drawn for the study of deformation behavior of mining slopes in mountainous areas with gentle anti-incline overburden rock strata:

(i) Mining in mountainous areas usually meets with the risk of slope instability. The overlying rock masses tended to move towards the sloping surface with mining beneath sloping terrain, which brought an asymmetrical subsidence funnel, and formed a wider relative disturbance range on the slope surface. In particular, the rock masses above the extracted panel were disturbed to the greatest with $D = 0$ m

(ii) The constraining forces of overburden rock masses towards the valley decrease; mining beneath sloping terrains usually acquire larger subsidence (up to 3 m) and additional horizontal displacement (up to 1.4 m) than flat terrains. The "zigzag" horizontal displacement change zone formed with the control of bedding planes

(iii) It is important to remain the center position of the extracted panel behind the slope shoulder, beyond which the deformation rate and ultimate value of the rock mass at the slope shoulder would increase drastically. In addition, the boundary of the extracted panel should also be avoided to cross over the slope shoulder (i.e., $D \leq -100$ m) to prevent an overall slope instability

Data Availability

The simulation codes and slope information used to support the findings of this study are available from the corresponding author upon request.

Conflicts of Interest

The authors declared that they have no conflicts of interest to this work. The authors declare that they do not have any commercial or associative interest that represents a conflict of interest in connection with the work submitted.

Acknowledgments

The authors would like to acknowledge the financial support from the State Key Laboratory of Geohazard Prevention and Geoenvironment Protection (Chengdu University of Technology) (Grant No. SKLGP2017Z016), the National Natural Science Foundation of China (Grant No. 41877273), the Innovative Research Groups of the National Natural Science Foundation of China (Grant No. 41521002), the Guizhou Provincial Geological Environment Monitoring Institute, and the Faer Coal Mine. These supports are gratefully acknowledged.

References

[1] A. Majdi, F. P. Hassani, and M. Y. Nasiri, "Prediction of the height of destressed zone above the mined panel roof in longwall coal mining," *International Journal of Coal Geology*, vol. 98, pp. 62–72, 2012.

[2] L. J. Donnelly, H. De La Cruz, I. Asmar, O. Zapata, and J. D. Perez, "The monitoring and prediction of mining subsidence in the Amaga, Angelopolis, Venecia and Bolombolo regions, Antioquia, Colombia," *Engineering Geology*, vol. 59, no. 1-2, pp. 103–114, 2001.

[3] M. Marschalko, I. Yilmaz, M. Bednárik, and K. Kubečka, "Influence of underground mining activities on the slope deformation genesis: Doubrava Vrchovec, Doubrava Ujala and Staric case studies from Czech Republic," *Engineering Geology*, vol. 147-148, pp. 37–51, 2012.

[4] E. F. Salmi, M. Nazem, and M. Karakus, "The effect of rock mass gradual deterioration on the mechanism of post-mining subsidence over shallow abandoned coal mines," *International Journal of Rock Mechanics and Mining Sciences*, vol. 91, pp. 59–71, 2017.

[5] H. G. Denkhaus, "Critical review of strata movement theories and their application to practical problems," *Journal of the Southern African Institute of Mining and Metallurgy*, vol. 64, no. 8, pp. 310–332, 1964.

[6] J. R. Dinsdale, "Ground pressure and pressure profiles around mining excavation," *Colliery Engineering*, vol. 12, pp. 406–409, 1935.

[7] M. R. Islam, D. Hayashi, and A. B. M. Kamruzzaman, "Finite element modeling of stress distributions and problems for multi-slice longwall mining in Bangladesh, with special reference to the Barapukuria coal mine," *International Journal of Coal Geology*, vol. 78, no. 2, pp. 91–109, 2009.

[8] M. M. Singh and F. S. Kendorski, "Strata disturbance prediction for mining beneath surface water and waste impoundments," in *Proceedings of the 1st Conference on Ground Control in Mining*, pp. 76–89, Morgantown, WV, USA, 1981.

[9] D. P. Sainsbury, B. L. Sainsbury, M. P. Board, and D. M. Loring, "Numerical back-analysis of structurally controlled cave initiation and propagation at the Henderson mine," in *45th US Rock Mechanics/Geomechanics Symposium*, p. 321, American Rock Mechanics Association, San Francisco, California, 2011.

[10] T. Unlu, H. Akcin, and O. Yilmaz, "An integrated approach for the prediction of subsidence for coal mining basins," *Engineering Geology*, vol. 166, pp. 186–203, 2013.

[11] B. Ghabraie, G. Ren, X. Zhang, and J. Smith, "Physical modelling of subsidence from sequential extraction of partially overlapping longwall panels and study of substrata movement characteristics," *International Journal of Coal Geology*, vol. 140, pp. 71–83, 2015.

[12] M. Karmis, A. Jarosz, P. Schilizzi, and Z. Agioutantis, "Surface deformation characteristics above undermined areas: experience from the eastern United States," *Civil Engineering Transactions*, vol. 29, no. 2, pp. 106–114, 1987.

[13] A. T. McCay, M. Valyrakis, and P. L. Younger, "A meta-analysis of coal mining induced subsidence data and implications for their use in the carbon industry," *International Journal of Coal Geology*, vol. 192, pp. 91–101, 2018.

[14] D. Zhang, G. Fan, L. Ma, and X. Wang, "Aquifer protection during longwall mining of shallow coal seams: a case study

in the Shendong Coalfield of China," *International Journal of Coal Geology*, vol. 86, no. 2-3, pp. 190–196, 2011.

[15] O. Düzgün, C. Künzer, and C. Özgen Karacan, "Applications of remote sensing and GIS for monitoring of coal fires, mine subsidence, environmental impacts of coal-mine closure and reclamation," *International Journal of Coal Geology*, vol. 86, no. 1, pp. 1-2, 2011.

[16] H. J. Oh and S. Lee, "Integration of ground subsidence hazard maps of abandoned coal mines in Samcheok, Korea," *International Journal of Coal Geology*, vol. 86, no. 1, pp. 58–72, 2011.

[17] E. Can, S. Kuşcu, and C. Mekik, "Determination of underground mining induced displacements using GPS observations in Zonguldak-Kozlu Hard Coal Basin," *International Journal of Coal Geology*, vol. 89, pp. 62–69, 2012.

[18] P. Hatherly, "Overview on the application of geophysics in coal mining," *International Journal of Coal Geology*, vol. 114, pp. 74–84, 2013.

[19] W.-d. Wu, J.-b. Bai, X.-y. Wang, Z.-j. Zhu, and S. Yan, "Field investigation of fractures evolution in overlying strata caused by extraction of the Jurassic and carboniferous coal seams and its application: case study," *International Journal of Coal Geology*, vol. 208, pp. 12–23, 2019.

[20] S. Zhang, X. Pei, S. Wang, R. Huang, X. Zhang, and Z. Chang, "Centrifuge model testing of a loess landslide induced by rising groundwater in Northwest China," *Engineering Geology*, vol. 259, article 105170, 2019.

[21] Y. G. Zhou, D. Meng, Q. Ma, B. Huang, D. S. Ling, and Y. M. Chen, "Centrifuge modeling of dynamic response of high fill slope by using generalized scaling law," *Engineering Geology*, vol. 260, p. 105213, 2019.

[22] Q. Bai, S. Tu, F. Wang, and C. Zhang, "Field and numerical investigations of gateroad system failure induced by hard roofs in a longwall top coal caving face," *International Journal of Coal Geology*, vol. 173, pp. 176–199, 2017.

[23] M. A. Coulthard and A. J. Dutton, "Numerical modelling of subsidence induced by underground coal mining," in *The 29th US Symposium on Rock Mechanics (USRMS)*, pp. 529–536, American Rock Mechanics Association, Minneapolis, Minnesota, 1988.

[24] M. Karmis, Z. Yu, and A. Jarosz, "Design considerations for subsidence control," *International Journal of Mining and Geological Engineering*, vol. 8, no. 4, pp. 357–368, 1990.

[25] L. J. Wardle and K. E. McNabb, "Three-dimensional numerical modelling of effects of subsidence on escarpments," in *Proceedings of the 11th International Congress On ground control in mining*, pp. 506–510, Wollongong, Australia, 1992.

[26] L. J. Wardle, "The use of numerical modeling for underground coal mine design," in *Analysis and Design Methods*, pp. 733–748, Pergamon, Oxford, UK, 1993.

[27] C. Zhang, R. Mitra, and B. Hebblewhite, "UDEC modeling of valley closure and upsidence," in *Continuum and Distinct Element Numerical Modeling in Geomechanics*, pp. 1–8, Itasca International Inc. Minneapolis, 2013.

[28] R. Bhasin and A. M. Kaynia, "Static and dynamic simulation of a 700-m high rock slope in western Norway," *Engineering Geology*, vol. 71, no. 3-4, pp. 213–226, 2004.

[29] E. F. Salmi and S. Hosseinzadeh, "Slope stability assessment using both empirical and numerical methods: a case study," *Bulletin of Engineering Geology and the Environment*, vol. 74, no. 1, pp. 13–25, 2015.

[30] M. Sharifzadeh, M. Sharifi, and S. M. Delbari, "Back analysis of an excavated slope failure in highly fractured rock mass: the case study of Kargar slope failure (Iran)," *Environment and Earth Science*, vol. 60, no. 1, pp. 183–192, 2010.

[31] P. J. N. Pells, "A note on escarpment instability associated with mining subsidence," in *Second Triennial Conference on Buildings and Structures Subject to Mine Subsidence*, pp. 66–73, Maitland, NSW, USA, 1991.

[32] P. J. N. Pells, J. C. Braybrooke, J. Mong, and G. P. Kotze, "Cliff line collapse associated with mining activities," in *Soil Slope Instability and Stabilisation*, pp. 359–385, Balkema, Rotterdam, Netherlands, 1987.

[33] A. Waddington and D. Kay, "The impacts of mine subsidence on creeks, river valleys and gorges due to underground coal mining operations," in *Proceedings of the 2003 Coal Operators Conference*, pp. 101–116, University of Wollongong & the Australasian Institute of Mining and Metallurgy Wollongong, Australasian, 2003.

[34] H. Zahiri, D. R. Palamara, P. Flentje, G. M. Brassington, and E. Baafi, "A GIS-based weights-of-evidence model for mapping cliff instabilities associated with mine subsidence," *Environmental Geology*, vol. 51, no. 3, pp. 377–386, 2006.

[35] M. Marschalko, I. Yilmaz, V. Křístková, M. Fuka, M. Bednarik, and K. Kubečka, "Determination of actual limit angles to the surface and their comparison with the empirical values in the upper Silesian Basin (Czech Republic)," *Engineering Geology*, vol. 124, pp. 130–138, 2012.

[36] J. J. Zhao, J. G. Xiao, M. L. Lee, and Y. T. Ma, "Discrete element modeling of a mining-induced rock slide," *SpringerPlus*, vol. 5, no. 1, p. 1633, 2016.

[37] D. B. Jones, H. J. Siddle, D. J. Reddish, and B. N. Whittaker, "Landslides and undermining: slope stability interaction with mining subsidence behaviour," in *7th ISRM Congress*, pp. 893–898, International Society for Rock Mechanics and Rock Engineering, Aachen, Germany, 1991.

[38] D. Page, *Mine Subsidence Devastates Sugarloaf: Video, Photos*, The NewcastleHerald, 2013.

[39] J. M. Galvin, *Ground Engineering-Principles and Practices for Underground Coal Mining*, Springer, 2016.

[40] J. E. Turney, A. Amundson, C. Greenman, B. K. Stover, and A. Bucknam, *Subsidence above Inactive Coal Mines: Information for the Homeowner*, Colorado Geological Survey, 1985.

[41] D. R. Kay, J. P. Barbato, and K. W. Mills, "Review of mechanisms resulting in observed upsidence and closure movements," in *Mine Subsidence 2007: Proceedings of the Seventh Triennial Conference on Mine Subsidence: A Community Issue-Mine Subsidence Technological Society*, pp. 197–205, University of Wollongong, Wollongong, 2007.

[42] D. R. Kay and J. P. Carter, *Effects of Subsidence on Steep Topography and Cliff Lines*, University of Sydney, Department of Architectural Science, 1992.

[43] D. M. Cunningham, "A rockfall avalanche in a sandstone landscape, Nattai North, NSW," *Australian Geographer*, vol. 19, pp. 221–229, 1988.

[44] I. Yilmaz and M. Marschalko, "A leaning historical monument formed by underground mining effect: an example from Czech Republic," *Engineering Geology*, vol. 133-134, pp. 43–48, 2012.

[45] J. Wei, Z. Zhao, C. Xu, and Q. Wen, "Numerical investigation of landslide kinetics for the recent Mabian landslide (Sichuan, China)," *Landslides*, vol. 16, no. 11, pp. 2287–2298, 2019.

[46] D. O. Potyondy and P. A. Cundall, "A bonded-particle model for rock," *International Journal of Rock Mechanics and Mining Sciences*, vol. 41, no. 8, pp. 1329–1364, 2004.

[47] C. Shi, D. Li, K. Chen, and J. Zhou, "Failure mechanism and stability analysis of the Zhenggang landslide in Yunnan Province of China using 3D particle flow code simulation," *Journal of Mountain Science*, vol. 13, pp. 891–905, 2016.

[48] E. T. Brown, "Estimating the mechanical properties of rock masses," in *Proceedings of the 1st Southern Hemisphere International Rock Mechanics Symposium (SHIRMS), Australian Centre for Geomechanics*, pp. 3–21, Perth, Australia, 2008.

[49] G. Wang, M. Wu, R. Wang, H. Xu, and X. Song, "Height of the mining-induced fractured zone above a coal face," *Engineering Geology*, vol. 216, pp. 140–152, 2017.

[50] E. F. Salmi, M. Nazem, and M. Karakus, "Numerical analysis of a large landslide induced by coal mining subsidence," *Engineering Geology*, vol. 217, pp. 141–152, 2017.

[51] K. W. Mills, "Developments in understanding subsidence with improved monitoring," in *Mine subsidence 2011: proceedings of the eighth triennial conference on Management of Subsidence. MineSubsidence Technological Society*, pp. 25–41, Sebel Kirkton Park, Hunter Valley, NSW, 2011.

[52] Y. F. Zou, "Research on calculation method of surface subsidence coefficient," *Chinese Journal of Geotechnical Engineering*, vol. 3, pp. 112–115, 1997.

[53] M. Khanal, D. Adhikary, C. Jayasundara, and R. Balusu, "Numerical study of mine site specific multiseam mining and its impact on surface subsidence and chain pillar stress," *Geotechnical and Geological Engineering*, vol. 34, no. 1, pp. 217–235, 2016.